

A hybrid plasmonic semiconductor laser

D. Costantini, L. Greusard, A. Bousseksou, Y. De Wilde, B. Habert et al.

Citation: *Appl. Phys. Lett.* **102**, 101106 (2013); doi: 10.1063/1.4794175

View online: <http://dx.doi.org/10.1063/1.4794175>

View Table of Contents: <http://apl.aip.org/resource/1/APPLAB/v102/i10>

Published by the [American Institute of Physics](#).

Related Articles

On the relationship between small and large signal modulation capabilities in highly nonlinear quantum dot lasers
Appl. Phys. Lett. **102**, 101107 (2013)

Continuous-wave coherent imaging with terahertz quantum cascade lasers using electro-optic harmonic sampling
Appl. Phys. Lett. **102**, 091107 (2013)

High-power InP quantum dot based semiconductor disk laser exceeding 1.3W
Appl. Phys. Lett. **102**, 092101 (2013)

Chirped InAs/InP quantum-dash laser with enhanced broad spectrum of stimulated emission
Appl. Phys. Lett. **102**, 091102 (2013)

Semiconductor laser monolithically pumped with a light emitting diode operating in the thermoelectrophotonic regime
Appl. Phys. Lett. **102**, 081116 (2013)

Additional information on *Appl. Phys. Lett.*

Journal Homepage: <http://apl.aip.org/>


Journal Information: http://apl.aip.org/about/about_the_journal

Top downloads: http://apl.aip.org/features/most_downloaded

Information for Authors: <http://apl.aip.org/authors>

ADVERTISEMENT

JANIS Does your research require low temperatures? Contact Janis today.
Our engineers will assist you in choosing the best system for your application.



10 mK to 800 K LHe/LN₂ Cryostats
Cryocoolers Magnet Systems
Dilution Refrigerator Systems
Micro-manipulated Probe Stations

sales@janis.com www.janis.com
Click to view our product web page.

A hybrid plasmonic semiconductor laser

D. Costantini,¹ L. Greusard,² A. Bousseksou,¹ Y. De Wilde,^{2,a)} B. Habert,³ F. Marquier,³ J.-J. Greffet,³ F. Lelarge,⁴ J. Decobert,⁴ G.-H. Duan,⁴ and R. Colombelli^{1,b)}

¹*Institut d'Electronique Fondamentale, Univ. Paris Sud, UMR8622 CNRS, 91405 Orsay, France*

²*Institut Langevin, ESPCI ParisTech, CNRS, 1, rue Jussieu, 75238 Paris Cedex 05, France*

³*Laboratoire Charles Fabry, Institut d'Optique, CNRS, Univ. Paris-Sud, 2 avenue Augustin Fresnel, 91127 Palaiseau cedex, France*

⁴*III-V Lab, Joint lab of Alcatel-Lucent Bell Labs France, Thales Research and Technology and CEA Leti, route de Nozay, 91461 Marcoussis cedex, France*

(Received 30 December 2012; accepted 20 February 2013; published online 13 March 2013)

We present a semiconductor-based approach to compensate plasmonic losses. The core idea is to employ an electrically pumped laser diode and to overlap its active region with the evanescent field of a surface plasmon wave. In order to keep the losses at a manageable level, we rely on hybrid waveguide modes stemming from the coupling of a dielectric and a plasmonic mode. The laser device we demonstrate operates—at telecom wavelengths—on such a hybrid plasmonic mode. The device operates by electrical injection at room temperature. The near-field imaging of the laser facet provides evidence of the stimulated emission into the hybrid mode and confirms the prediction of the numerical simulations. © 2013 American Institute of Physics. [<http://dx.doi.org/10.1063/1.4794175>]

Surface plasmon polaritons (SPPs) are interface electromagnetic modes between a metal and a dielectric. The field—maximal at the interface—decays exponentially in both media.¹ A distinctive characteristic of SPPs is the possibility to achieve sub-wavelength light concentration.^{2,3} They find use in a variety of applications⁴ but meet a limit in their typically large optical losses. Recently, efforts have been dedicated to overcome such losses⁵ in order to enable real-world applications of plasmonic technology.⁶

A full compensation of plasmonic losses at telecom wavelengths is a formidable task: for a SPP propagating, at $\lambda = 1.3\mu\text{m}$, along the interface between air and gold ($n_{\text{air}} = 1$ and $n_{\text{gold}} = 0.403 + i8.25$, Ref. 7), losses are estimated to be only 80 cm^{-1} . However, compensating the SPP losses requires replacing air with a gain medium that is necessary denser and has higher optical index. Plasmonic losses roughly scale with the optical index of the dielectric to the 3rd power,¹ leading to prohibitively high values. For instance, more than 2000 cm^{-1} are obtained for an interface between a dielectric with $n = 3$ and gold ($\lambda = 1.3\mu\text{m}$). Even with state-of-the-art semiconductor active regions (ARs), which represent one of the best available gain media, gain values that can compensate such losses are unattainable. For plasmonic nano-lasers, it has been estimated that net amplification would require current densities of more than 100 kA/cm^2 (see Ref. 8). A viable trade-off for full loss compensation is to rely on hybrid waveguide modes stemming from the coupling of a dielectric and a plasmonic mode.⁹ A hybrid mode presents advantageously lower losses compared to a pure SPP and it allows, at the same time, a good overlap with the gain medium.¹⁰ Furthermore hybrid modes—in the proper configuration—exhibit high field intensities in a sub-wavelength space. Most of the proposed amplifiers relying on hybrid modes, among them the nanolasers,^{11–13} are optically pumped or operate at low temperature.¹⁴ Electrically pumped

devices operating at room temperature (RT) are a necessary evolution for applications.

In the first part of this paper, the concept of hybrid plasmonic mode is developed. We then turn to our specific device case (ridge geometry) and present the associated 1D and 2D simulations. The core of the paper focuses on the electrical and optical device characterization, including—importantly—the near-field images of the laser facets which allow one to directly visualize the hybrid mode.

The semiconductor device we introduce operates by electrical injection and it is based on standard ridge-waveguide geometry, with light emitted from the cleaved facets. The hybrid mode stems from the coupling between (i) a classical transverse magnetic (TM) polarized mode guided within the active region (AR) by the dielectric claddings and (ii) a SPP mode, guided at the interface between the upper cladding and the top metal contact of the device (Fig. 1(a)). The coupling strength between the two modes depends on the materials index of refraction, the ridge width, and can be precisely tuned with the upper cladding thickness (t_{cl}). Large cladding thicknesses lead to uncoupled “dielectric” and “plasmonic” modes (Fig. 1(b)). Instead, when t_{cl} is comparable to the modes extent, hybrid modes appear thanks to their overlap (Fig. 1(c)). The hybrid modes obviously present both “dielectric” and “plasmonic” characters and can be labeled as symmetric and anti-symmetric, according to the relative sign of the two components. The relative weight of the plasmonic/dielectric components of the hybrid modes is set in a more indirect way and can be deduced from the uncoupled dispersion relations. The “closer” the dispersion relations are, the stronger the mode hybridization is. Some systems allow a crossing of the two uncoupled dispersions (see for instance Ref. 15 for a coupling between a long range surface plasmon waveguide and a dielectric one). In that case, the dispersions of the coupled modes show a typical “anti-crossing” behavior, where both hybridized modes have an equal repartition of dielectric and plasmonic characters. Far from this region, the modes are

^{a)}E-mail: yannick.dewilde@espci.fr.

^{b)}E-mail: raffaele.colombelli@u-psud.fr.

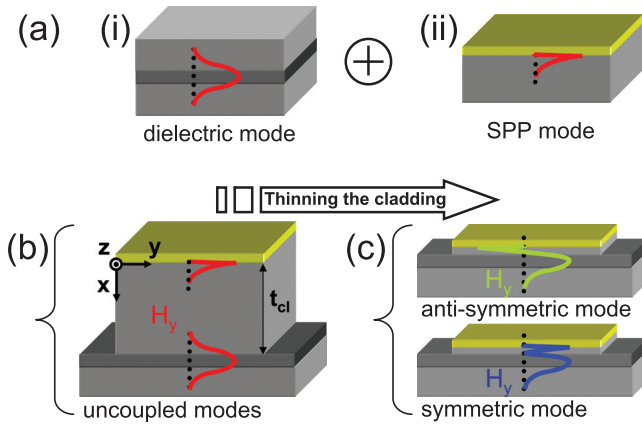


FIG. 1. (a) Schematics of the magnetic field distribution (H_y component) of the two waveguided modes: (i) the dielectric mode confined in the AR and (ii) the SPP mode at the metal-semiconductor interface. (b) The two modes on the same ridge. They are not coupled since the thick (t_{cl}) upper cladding prevents the coupling. (c) A thin cladding enables mode coupling, yielding two hybrid modes (one symmetric and one anti-symmetric). They both present a “plasmonic” and a “dielectric” component. The electric field is traditionally employed to describe the laser modes. We plot here the magnetic field instead in order to highlight the symmetric/anti-symmetric character of the modes.

mostly plasmonic-like or dielectric-like. The anti-crossing existence is determined by the system geometry and the used materials, namely by the material indexes and ridge widths. In our case, the dispersion relations do not cross, but—as discussed later—are sufficiently close to yield a measurable hybridization. This is actually an advantage, since a perfect “anti-crossing” situation would lead to two extremely high-loss modes. They would both be half “plasmonic,” exhibiting losses dominated by the extremely damped “plasmonic” component. Instead, if the dispersions do not cross—as in our case—it is possible to tune the coupling between the modes, modifying the dispersion diagrams at the laser operating frequency and consequently to engineer the mode losses. Putting the gain region in direct contact with the metal is not possible, since the upper cladding plays the necessary role of charge reservoir for the pn junction. In this paper, we will reduce its thickness to the minimum possible value in order to enhance the plasmonic character of the hybrid mode.

The active region (AR) used is an InP-based laser diode operating at telecom wavelength ($\lambda = 1.3\mu\text{m}$) by electrical injection. The AR is composed of 9 tensile-strained quantum wells (QWs)¹⁶ whose optical emission is TM polarized light. This AR also provides a very high differential gain.¹⁷ The detailed structure is reported in Table I. The upper cladding is constituted of a 100-nm-thick highly doped contact layer (unavoidable for efficient charge injection), a p-doped InP layer (x nm), and a 50-nm-thick non-intentionally doped InP layer. We realized devices with different thicknesses of the p-doped InP layer, thus tuning the plasmonic character of the hybrid-modes

- $x = 2650$ nm, ($t_{cl} = 2800$ nm),
- $x = 300$ nm, ($t_{cl} = 450$ nm),
- $x = 100$ nm, ($t_{cl} = 250$ nm).

Each upper cladding was grown on identical active regions by molecular beam epitaxy (MBE). The devices

TABLE I. Detailed description of the structure, with material, thickness, doping, and optical index of each layer. The AR is grown by metal-organic chemical vapor deposition (MOCVD), while the upper cladding is grown by MBE.

Layer type	Material	Thickness (nm)	Doping (cm^{-3})	Optical index
Metal	Au (gold)	200		$0.403 - i8.25$
Contact layers	InGaAs	15	2×10^{19}	3.34
	InGaAsP	80	2×10^{19}	3.34
Claddings	InP	x	1.4×10^{18}	$3.2 - i5.93 \times 10^{-4}$
	InP	50	n.i.d.	3.2
Active region	InGaAlAs	300	n.i.d.	3.45
Substrate	InP	2×10^3	-1×10^{18}	$3.2 - i1.36 \times 10^{-5}$

were processed into 9- μm -wide, 750- μm -long mesa etched ridges. Electrical insulation was provided by a 300-nm-thick SiN layer which was opened above the ridges before the top metal contact evaporation. A thin Ti-sticking layer was employed for the devices with $t_{cl} = 2800$ nm and $t_{cl} = 450$ nm before the top gold deposition. In contrast, we did not employ it for the thinnest device ($t_{cl} = 250$ nm) for loss-control purposes. In fact, the electric field at the metallic interface in these devices is so intense that simulations predict a dramatic loss increase of $\approx 170 \text{ cm}^{-1}$ with only 3-nm of Ti.¹⁸

Figure 2(a) reports the calculated dispersion curves of a structure with $t_{cl} = 250$ nm obtained with 1D simulations.¹⁹ The color code corresponds to the scheme in Fig. 1(c) for ease of reading. The uncoupled mode dispersions (red dots) do not cross, hence only a small shift is expected upon coupling, as highlighted in the picture inset. At $\lambda = 1.3\mu\text{m}$, the hybrid modes (green and blue lines) exhibit a slightly modified wavevector. Note that the anti-symmetric hybrid mode (green line) presents a plasmonic component which is smaller compared to the symmetric hybrid mode. This perturbative regime allows the anti-symmetric mode to have a plasmonic component, but at the same time, a good overlap with the AR (= 53%) and with acceptable total optical losses ($\alpha \approx 500 \text{ cm}^{-1}$). On the other hand, the symmetric mode exhibits huge losses ($\alpha \geq 6000 \text{ cm}^{-1}$), which cannot be compensated by gain. The laser cannot, therefore, operate on the symmetric mode. A 2D finite element simulation²⁰ of the ridge frontal section displaying the electric-field (squared norm) distribution of the anti-symmetric mode at $\lambda = 1.3\mu\text{m}$ is presented in Fig. 2(b). The central, 1D cross-section quantifies the plasmonic component at about 30% of the mode maximum.

All the devices operate at RT in pulsed mode. The device with $t_{cl} = 2800$ nm can operate in CW too. Figure 3(a) reports typical light-current density (LJ) characteristics of the three devices in pulsed regime. The devices exhibit a clear laser effect, as proven by the typical non linear threshold behavior of the LJ curve. The threshold current density increases as follows upon t_{cl} reduction:

- 1.5 kA/cm^2 for $t_{cl} = 2800$ nm (simulated losses = 5 cm^{-1}),
- 3 kA/cm^2 for $t_{cl} = 450$ nm (simulated losses = 140 cm^{-1}),

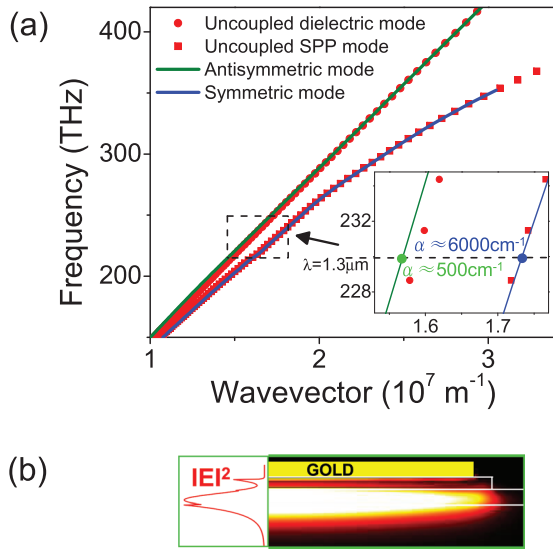


FIG. 2. (a) Mode dispersion curves for a real structure with a 250-nm-thick cladding, calculated using a finite elements 1D simulation. The gold index dispersion is taken from Ref. 7. The dispersions of the uncoupled modes do not cross: the mode coupling induces only slight perturbation, which is best visible in the inset. The advantage is the onset of a hybrid, relatively low-loss mode, which is highlighted by a green point in the inset. (b) Finite elements simulation of the low-loss hybrid waveguided mode for a laser with a 250-nm-thick cladding ($\lambda = 1300$ nm). The electric field squared modulus is plotted and a 1D cross-section is shown on the left. The maximum of the “plasmonic” component is about 30% of the mode maximum. The propagation loss is $\alpha \approx 500$ cm^{-1} .

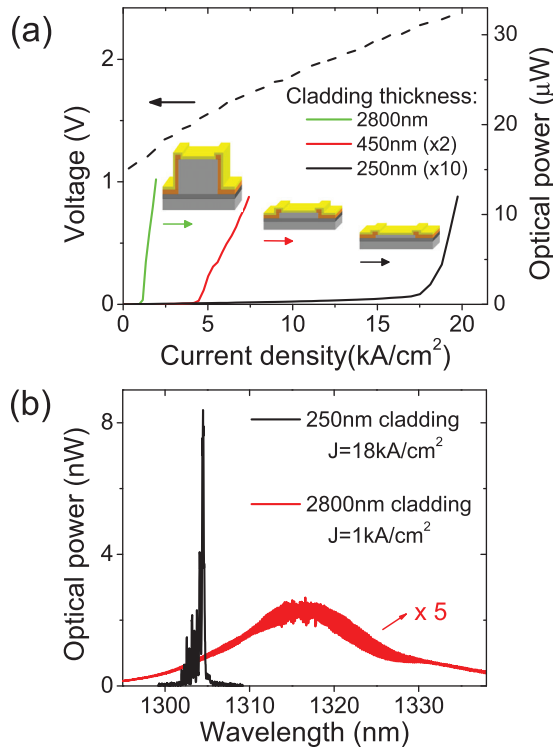


FIG. 3. LJ curves, in pulsed regime (DC=1%—10kHz repetition rate, 100 ns pulses), for three ridges with different cladding thicknesses: $t_{cl} = 2800$ nm (green curve), $t_{cl} = 450$ nm (red curve), and $t_{cl} = 250$ nm (black curve). Reducing the cladding thickness brings the metal closer to the AR, hence increasing optical losses and laser thresholds. The JV characteristic (dashed black line) is also shown for a device with $t_{cl} = 250$ nm. (b) Typical laser spectrum (black line) of a device with $t_{cl} = 250$ nm at an injection current density of 18 kA/cm^2 . Luminescence spectrum (red line) of a device with $t_{cl} = 2800$ nm at $J = 1$ kA/cm^2 .

- $17 \text{ kA}/\text{cm}^2$ for $t_{cl} = 250$ nm (simulated losses = 480 cm^{-1}).

Although the ratio between the calculated losses of the device with $t_{cl} = 250$ nm and $t_{cl} = 450$ nm is about 3.5; the ratio of the experimental laser thresholds exceeds five. This behavior is typical of diode lasers: the differential gain is not constant with the injected current density,¹⁷ but it has instead a logarithmic dependence. We assume that even for $t_{cl} = 250$ nm, no gain quenching is occurring. The latter would be relevant for distances between gain and metal of the order of 20 nm (Ref. 22). Figure 3(b) shows the laser RT spectrum of the thinnest device, which correctly emits at $\lambda = 1.3 \mu\text{m}$. As a further corroborating evidence of stimulated emission, the comparison with an electro-luminescence spectrum of the thickest device allows one to appreciate the spectral narrowing of the emission when the device operates in the lasing regime.

An original feature of the present work is the characterization of the plasmonic hybrid mode by near-field scanning optical microscopy (NSOM), which allowed us to directly visualize the field distribution while the laser is operating. The NSOM setup is based on a commercial Witec aperture microscope which has been adapted at telecom wavelengths (details in Ref. 21). The results of the NSOM analysis of the device facets are shown in Fig. 4. For each device, we report the SEM image and the associated electromagnetic near field collected above laser threshold (see Figs. 4(a)–4(c) (Ref. 23)). A quantitative data analysis was performed by integrating the NSOM signal along the y-direction. The cross-section is spatially averaged along $\approx 4 \mu\text{m}$ in the y direction, with steps of 100 nm. Each normalized integral curve is plotted in Figs. 4(d)–4(f) (red lines) with the corresponding numerically simulated cross-sections of $|\mathbf{E}|^2$ (black lines). The dielectric components are in excellent agreement with the simulations and for the two devices with thinnest claddings, we observe a clear NSOM signal in correspondence of

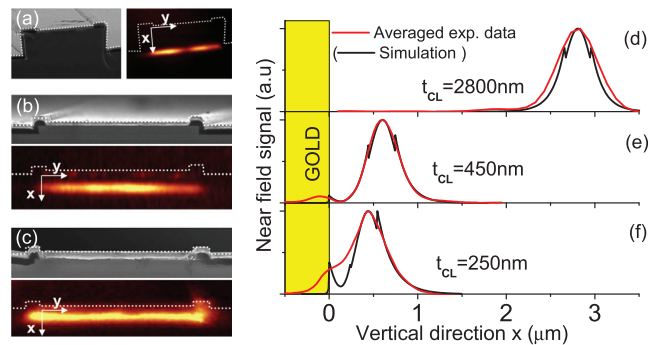


FIG. 4. (a)–(c): SEM images and NSOM measurement of the facets for three different laser types: (a) $t_{cl} = 2800$ nm, (b) $t_{cl} = 450$ nm, and (c) $t_{cl} = 250$ nm. The lasing mode can be clearly identified and positioned with respect to the facet. (d)–(f): Integrated NSOM signal (red lines, integration performed along the y-direction) and square of the electric field (black line) obtained from 2D finite element simulations. The origin of the x coordinate is taken at the metal-semiconductor interface and the curves are normalized. The agreement between experiment and theory is good, taking into account a tip-induced broadening of the NSOM data, which prevents the system from detecting the extremely sharp decrease in field at the metal-semiconductor interface. See also note in Ref. 23.

the gold/semiconductor interface. It corresponds to the plasmonic component of the hybrid-mode, which takes advantage of the optical gain experienced by the dielectric portion (which overlaps the AR), hence providing a clearly measurable field intensity at the metal-semiconductor interface. The plasmonic component in the NSOM measurement is broadened by the finite diameter ($d \approx 100$ nm) of the hole of the aluminum pyramid used in the Witec microscope. The measurement takes into account the total signal coming from a surface of $\pi(d/2)^2$, hence smoothing the abrupt extinction of the plasmonic component at the interface. Additional broadening possibly arises from the diffusion of the SPP at the facet level, where the roughness of the cleaved gold layer prevents a perfect contact-mode of the NSOM pyramid during the scanning of the interface. Nevertheless the intensity peak of the optical signal at the interface is well reproduced by the simulations (for $t_{cl} = 250$ nm, it is one third of the mode maximum). This confirms the plasmonic character of the hybrid mode which is lasing at room-temperature and upon electrical injection.

We have demonstrated a hybrid plasmonic laser emitting at telecom wavelengths. The device presents the advantages of the electrical injection and the operation at room temperature. Near-field microscopy measurements allowed us to directly measure the mode distribution and to prove the presence of the lasing plasmonic component. We believe that a fundamental study of the metal proximity to a gain media, combined with the electrical injection, represents an important step toward the development of active plasmonic components.

We thank A. Degiron for useful discussions. The device fabrication has been performed at the nano-center CTU-IEF-Minerve. This work was supported by the French National Research Agency (ANR-09-NANO-020 GOSPEL), from the Triangle de la Physique (Project PHLARE) and by the région Ile de France through a C’Nano IdF project. L.G. acknowledges support from the Direction Générale de l’Armement (DGA).

- ¹H. Raether, *Surface Plasmons on Smooth and Rough Surfaces and on Gratings* (Springer, Berlin, 1988).
- ²J. A. Schuller, E. S. Barnard, W. Cai, Y. C. Jun, J. S. White, and M. L. Brongersma, *Nature Mater.* **9**, 193 (2010).
- ³D. K. Gramotnev and S. I. Bozhevolnyi, *Nat. Photonics* **4**, 83 (2010).
- ⁴M. I. Stockman, *Phys. Today* **64**(2), 39 (2011).
- ⁵P. Berini and I. De Leon, *Nat. Photonics* **6**, 16 (2011).
- ⁶T. W. Ebbesen, C. Genet, and S. I. Bozhevolnyi, *Phys. Today* **61**(5), 44 (2008).
- ⁷E. D. Palik, *Handbook of Optical Constants of Solids* (Academic, 1998).
- ⁸J. B. Khurgin and G. Sun, *Appl. Phys. Lett.* **100**, 011105 (2012).
- ⁹R. F. Oulton, V. J. Sorger, D. A. Genov, D. F. P. Pile, and X. Zhang, *Nat. Photonics* **2**, 496 (2008).
- ¹⁰A. Christ, S. G. Tikhodeev, N. A. Gippius, J. Kuhl, and H. Giessen, *Phys. Rev. Lett.* **91**, 183901 (2003).
- ¹¹R. F. Oulton, V. J. Sorger, T. Zentgraf, R.-M. Ma, C. Gladden, L. Dai, G. Bartal, and X. Zhang, *Nature* **461**, 629 (2009).
- ¹²R.-M. Ma, R. F. Oulton, V. J. Sorger, G. Bartal, and X. Zhang, *Nature Mater.* **10**, 110 (2011).
- ¹³R. A. Flynn, C. S. Kim, I. Vurgaftman, M. Kim, J. R. Meyer, A. J. Mäkinen, K. Bussmann, L. Cheng, F.-S. Choa, and J. P. Long, *Opt. Express* **19**, 8954 (2011).
- ¹⁴M. T. Hill, M. Marell, E. S. P. Leong, B. Smalbrugge, Y. Zhu, M. Sun, P. J. van Veldhoven, E. J. Geluk, F. Karouta, Y.-S. Oei, R. Nötzel, C.-Z. Ning, and M. K. Smit, *Opt. Express* **17**, 11107 (2009).
- ¹⁵A. Degiron, S.-Y. Cho, T. Tyler, N. M. Jokerst, and D. R. Smith, *New J. Phys.* **11**, 015002 (2009).
- ¹⁶J. Decobert, N. Lagay, C. Cuisin, B. Dagens, B. Thedrez, and F. Laruelle, *J. Cryst. Growth* **272**, 543 (2004).
- ¹⁷D. Costantini, A. Bousseksou, M. Fevrier, B. Dagens, and R. Colombelli, *IEEE J. Quantum Electron.* **48**, 73 (2012).
- ¹⁸These thinnest structures were fabricated depositing a gold layer after the insulator opening and then encapsulating it with the standard evaporation of the top metal layer (ti/au). The encapsulation process guarantees a robust device and avoids the removal of the first gold layer.
- ¹⁹Fimmwave software, Photon Design, Oxford, UK.
- ²⁰COMSOL: MULTIPHYSICS finite element analysis simulation software, COMSOL Inc.
- ²¹D. Costantini, L. Greusard, A. Bousseksou, R. Rungsawang, T. P. Zhang, S. Callard, J. Decobert, F. Lelarge, G.-H. Duan, Y. De Wilde, and R. Colombelli, *Nano Lett.* **12**, 4693 (2012).
- ²²I. De Leon and P. Berini, “Theory of surface plasmon-polariton amplification in planar structures incorporating dipolar gain media,” *Phys. Rev. B* **78**, 161401 (2008).
- ²³Note: A careful observation of Fig. 4(c) reveals that the optical signal is slightly leaking on the right side of the ridge. This suggests the necessity, for extremely thin cladding structures, of maximizing the metal coverage along the ridge width, to avoid undesired low-threshold lateral modes. As visible in the SEM image, we have optimized the ridge fabrication in this sense.